Electronic Supplementary Information for:

Cobalt and Vanadium Co-doped FeOOH Nanoribbons: An Iron-rich Electrocatalyst for Efficient Water Oxidation

Xin Wang[a, ‡], *Wei Liu*[a, ‡, *], *Jingnan Wang*[a], *Chuanming Li*[a], *Rongkun Zheng*[a], *Hongxiu Zhang*[a], *Jingquan Liu*[a, *], *and Xingwang Zhang*[b, *]

[a] College of Materials Science and Engineering, Linyi University, Linyi276000, Shandong, China.

[b] College of Chemical and Biological Engineering, Zhejiang University, Hangzhou 310027, Zhejiang, China.

E-mail: liuweicl@lyu.edu.cn; jliu@qdu.edu.cn; xwzhang@zju.edu.cn

Contents

I. Experiment Section

Materials: Nickel foam and iron foam (1 mm, thickness) were purchased from Kunshan Jiayisheng Electronic Co., Ltd (Kunshan, China). VCl_3 and $CoCl_2 \cdot 6H_2O$ were got from Shanghai Macklin Biochemical Co., Ltd. KOH was purchased from Aladdin. Deionized (DI) water was used to prepare aqueous solutions and wash the samples.

Synthesis of (Co,V)-FeOOH on Ni foam: Prior to use, a piece of Ni foam (NF, with a length of 20 mm and a width of 5 mm) was cleaned by ultrasound in acetone, 1 M HCl, ethanol, and then DI water for 30 min, respectively. In a typical synthesis of (Co,V)-FeOOH/NF, 20 mL of NaCl (1 M), 18.2 mL of $CoCl_2 \cdot 6H_2O$ (5 mM) and 1.8 mL of VCl_3 (5 mM) were injected into an electrolyzer and was magnetically stirred for several minutes to form a homogenous solution. Then the pretreated NF and fresh iron foam (IF) were immersed in the above solution and connected to each other by conducting wire. After 8 hours of reaction, the sample of (Co,V)-FeOOH /NF was taken out and rinsed with DI water for several times. A series of reference samples, FeOOH, Co-doped FeOOH (Co-FeOOH), V-doped FeOOH (V-FeOOH) and Co/V co-doped FeOOH ((Co,V)-FeOOH) were synthesized by the similar procedure. The doping contents of foreign Co and V atoms in the host structure of FeOOH can be regulated by adjusting the molar ratio of Co/V ions in the homogenous solution, while maintaining the total amount of Co^{2+} and V^{3+}ions as 0.1 mmol.

Structure characterization: SEM images were obtained on an SU-80 (Hitachi) microscope at the accelerating voltage of 20 kV. TEM, HRTEM and the

corresponding elemental mappings were performed on Tecnai G2 F20 S-TWIN microscope. A Shimadzu XRD-6000 X-ray diffractometer furnished with Cu Kα radiation was used to collect the data of XRD. AFM image was obtained on a DI Innova Multimode SPM platform. XPS spectra were obtained on an Escalab 250Xi using Mg Kα radiation. XPS results were caliberated by setting binding energy of C 1s peak to 284.8 eV.

Electrochemical measurements: All the electrochemical measurements were conducted on a CHI 660E potentiostat with a standard three-electrode system. The as-prepared samples grown on NF (5×5 mm^2) were used as working electrodes. The Hg/HgO electrode and graphite rod as reference electrode and counter electrode, respectively. All measured potentials were converted to reversible hydrogen electrode (RHE). The linear sweep voltammetry (LSV) curves were obtained at a scan rate of 10 mV s^{-1} with iR correction. All EIS measurements were performed at 0.6 V vs. Hg/HgO with the frequency from to 0.01 Hz to 100 kHz. The double-layer capacitance (C_{dl}) values were derived from the cyclic voltammograms (CVs) at various scan rates.

Computational methods

The structure of pristine FeOOH was derived from the previous study, and the (010) facet of FeOOH is chosen because it is the most accessible and lowest energy facet for FeOOH[S1].We have employed the first-principles to perform all Spin-polarization density functional theory (DFT) calculations within the generalized gradient approximation (GGA) using the Perdew-Burke-Ernzerhof (PBE)

formulation[S2-S4]. We have chosen the projected augmented wave (PAW) potentials to describe the ionic cores and take valence electrons into account using a plane wave basis set with a kinetic energy cutoff of 400 eV[S5,S6]. Partial occupancies of the Kohn−Sham orbitals were allowed using the Gaussian smearing method and a width of 0.05 eV. The electronic energy was considered self-consistent when the energy change was smaller than 10^{-6} eV. A geometry optimization was considered convergent when the energy change was smaller than 0.05 eV $Å^{-1}$. In addition, for the Fe, Ni and V atoms, the U schemes need to be applied, and the U has been set as 3.44, 3.21 and 2.92 eV. The ΔG for each step in our OER steps can be calculated by:

$\Delta G_1 = G(OH^*) + G(H^+ + e^-) - G(H_2O) - G(^*)$

$= \{\Delta G_{OH^*} + G(^*) + [G(H_2O) - 1/2G(H_2)]\} + 1/2G(H_2) - G(H_2O) - G(^*)$

$= \Delta G_{OH^*}$

$\Delta G_2 = G(O^*) + G(H^+ + e^-) - G(OH^*)$

$= \{\Delta G_{O^*} + G(^*) + [G(H_2O) - G(H_2)]\} + 1/2G(H_2) - \{\Delta G_{OH^*} + G(^*) + [G(H_2O) - 1/2G(H_2)]\}$

$= \Delta G_{O^*} - \Delta G_{OH^*}$

$\Delta G_3 = G(OOH^*) + G(H^+ + e^-) - G(O^*) - G(H_2O)$

$= \{\Delta G_{OOH^*} + G(^*) + [2G(H_2O) - 3/2G(H_2)]\} + 1/2G(H_2) - \{\Delta G_{O^*} + G(^*) + [G(H_2O) - 1G(H_2)]\} - G(H_2O)$

$= \Delta G_{OOH^*} - \Delta G_{O^*}$

$\Delta G_4 = G(O_2) + G(H^+ + e^-) - G(OOH^*)$

$= \{4.92 + 2G(H_2O) - 2G(H_2)\} + 1/2G(H_2) - \{\Delta G_{OOH^*} + G(^*) + [2G(H_2O) - 3/2G(H_2)]\}$

$= 4.92 - \Delta G_{OOH^*}$

Then the free energies can be obtained by including the zero point energy (ZPE) and the entropy (S) corrections in equation $G = E_{ads}+ZPE-TS$, The ZPE could be obtained from the calculation of vibrational frequencies for the adsorbed species.

II. LSV of samples with various reaction time and molar ratios of Co/V

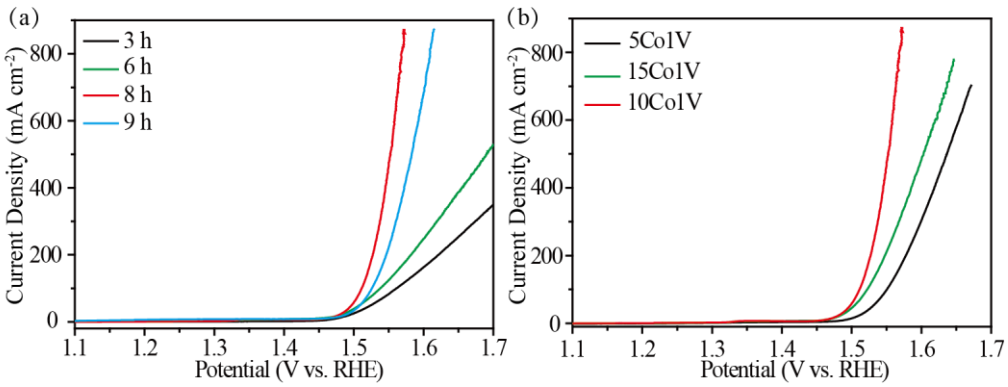

Figure S1. (a) Polarization curves for OER of samples with various reaction times in 1 M KOH with a scan rate of 10 mV s^{-1}. All samples were prepared with a Co/V ratio of 10:1 in the precursor solution. (b) Polarization curves for OER of samples with various molar ratios of Co/V in the precursor solution with a scan rate of 10 mV s^{-1}. In the xCoyV expression, the x and y represent the molar ratios of Co/V in the precursor solution. All samples were prepared with a reaction time of 8 hours.

III. XRD patterns of FeOOH and Co and/or V doped FeOOH

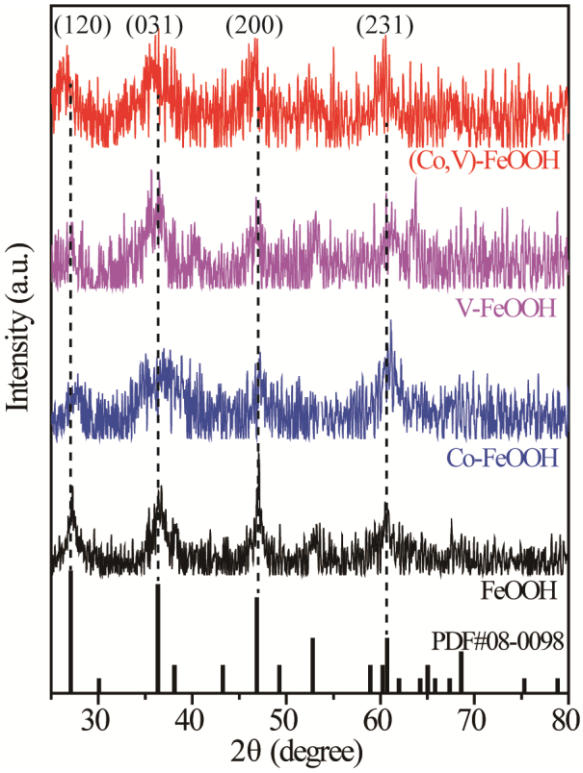

Figure S2. XRD patterns of the as-prepared FeOOH, Co-FeOOH, V-FeOOH and (Co,V)-FeOOH catalysts.

IV. The typical SEM images of FeOOH

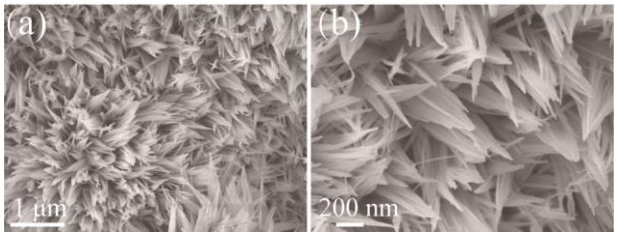

Figure S3. SEM images of the as-prepared FeOOH catalyst with low (a) and high (b) magnifications.

V. The typical SEM images of Co-FeOOH and V-FeOOH

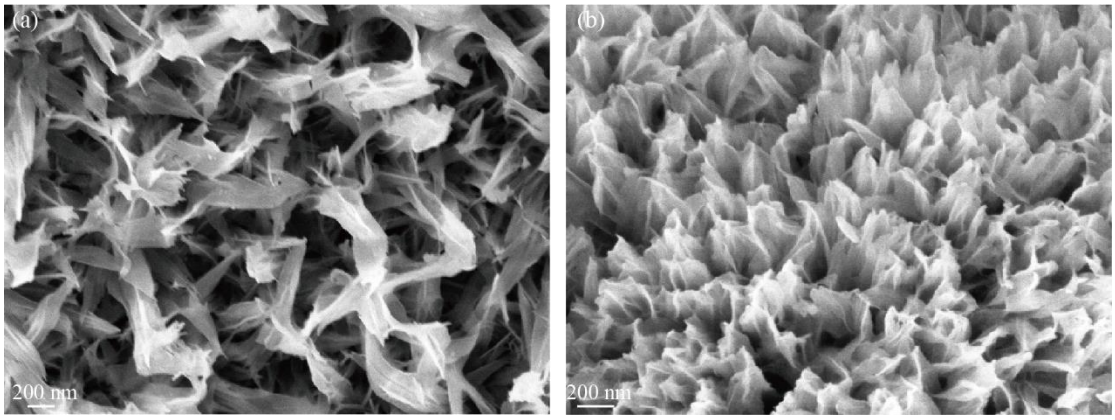

Figure S4. The typical SEM image of Co-FeOOH (a) and V-FeOOH (b).

VI. The typical SEM images of nickel foam (NF)

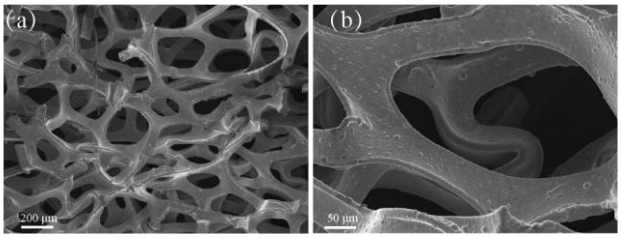

Figure S5. SEM images of the pristine NF with low (a) and high (b) magnifications.

VII. AFM and line-scan profiles of (Co,V)-FeOOH

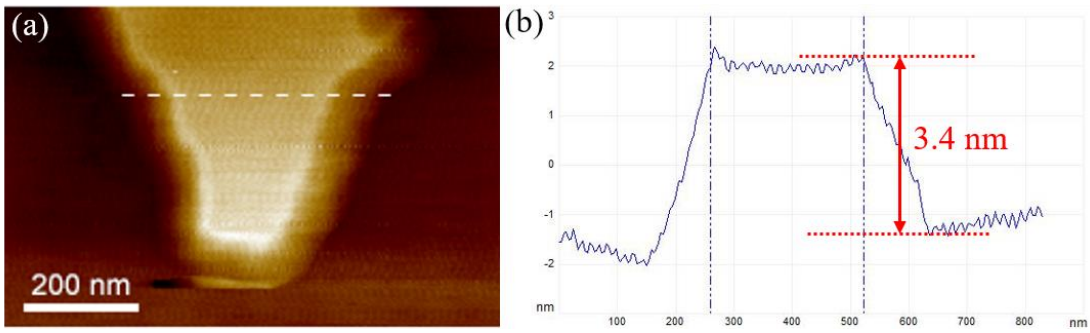

Figure S6. (a) AFM image and (b) line-scan profiles of (Co,V)-FeOOH.

VIII. HRTEM, HAADF-STEM and EDX image of the FeOOH catalyst

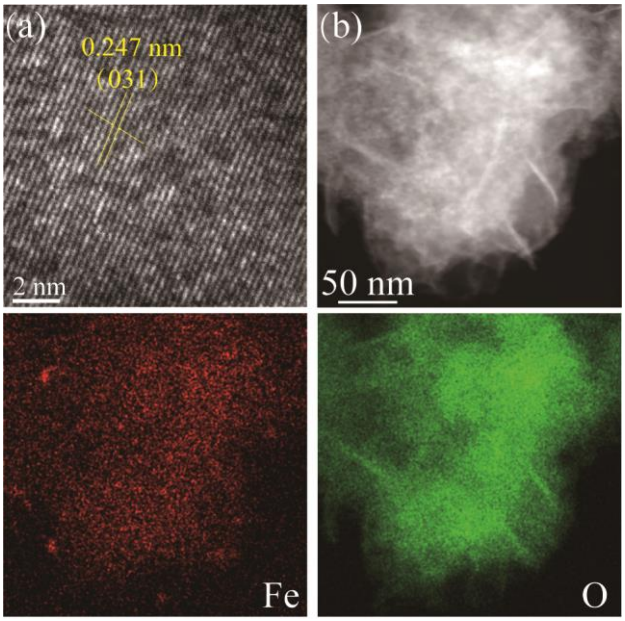

Figure S7. (a) HRTEM image of the as-prepared FeOOH catalyst. (b) HAADF-STEM image of FeOOH, the corresponding EDX elemental mappings of Fe and O.

IX. The survey XPS spectra of FeOOH and (Co,V)-FeOOH

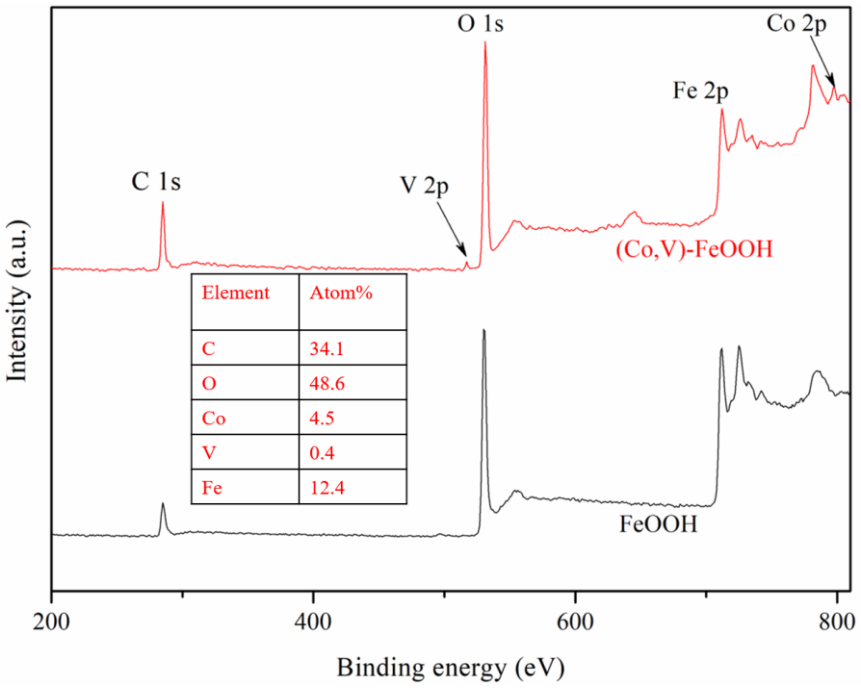

Element	Atom%
C	34.1
O	48.6
Co	4.5
V	0.4
Fe	12.4

Figure S8. The survey XPS spectra of FeOOH and (Co,V)-FeOOH.

X. Raman spectra of FeOOH and (Co,V)-FeOOH

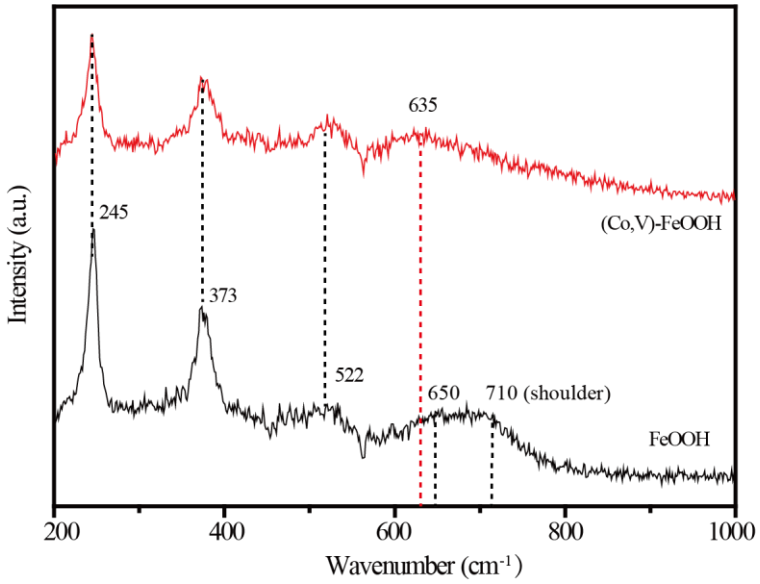

Figure S9 Raman spectra of FeOOH and (Co,V)-FeOOH.

XI. Current density of various samples at the overpotential of 322 mV

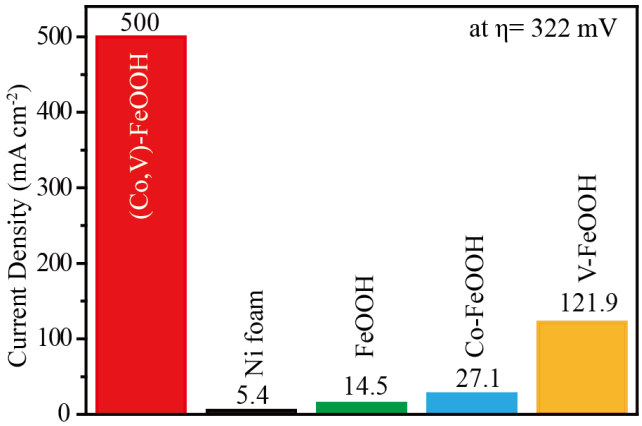

Figure S10 Current density of (Co,V)-FeOOH, Ni foam, FeOOH, Co-FeOOH and V-FeOOH at the overpotential of 322 mV.

XII. Cyclic voltammograms and C_{dl} for various samples

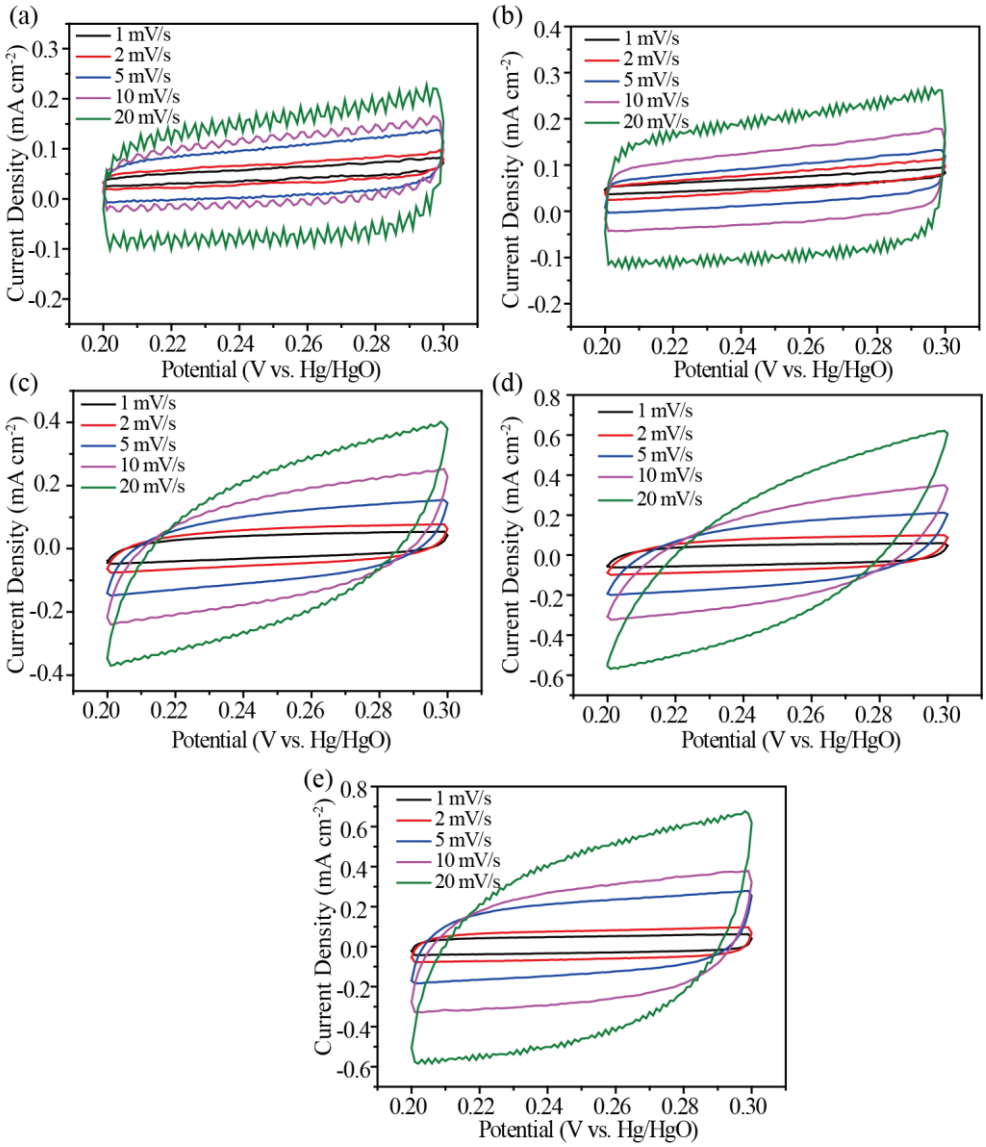

Figure S11. Cyclic voltammograms at different scan rates of 1, 2, 5, 10 and 20 mV s^{-1} for (a) Ni foam, (b) FeOOH, (c) Co-FeOOH, (d) V-FeOOH, and (e) (Co,V)-FeOOH.

XIII. Density of states (DOS) of FeOOH, Co-FeOOH and V-FeOOH

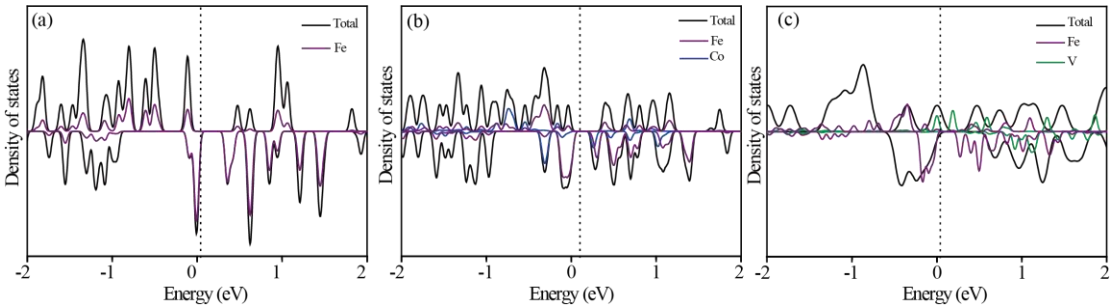

Figure S12. Density of states (DOS) of (a) FeOOH, (b) Co-FeOOH, and (c) V-FeOOH model, respectively.

XIV. Structure representations of FeOOH, Co-FeOOH and V-FeOOH

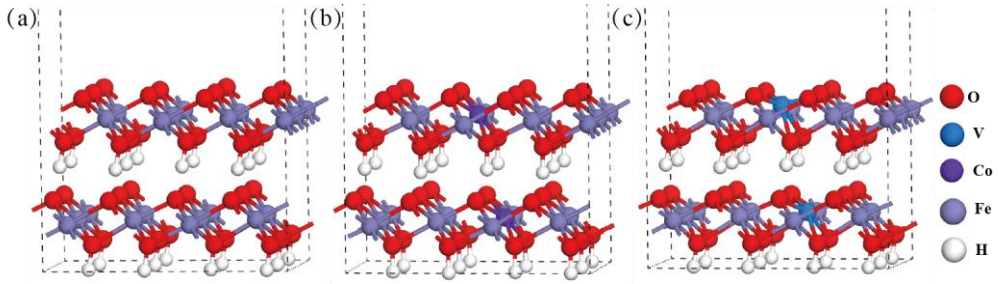

Figure S13. Structure representations of (a) FeOOH, (b) Co-FeOOH, and (c) V-FeOOH. O atoms are presented in red, V in blue, Co in purple, Fe in gray, and H in white.

XV. Structures of intermediates adsorbed on Fe site in FeOOH

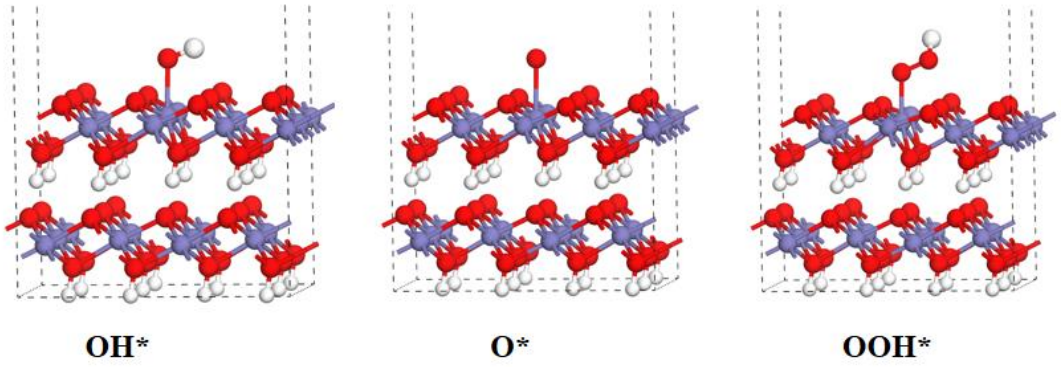

Figure S14. Structures of an OH*, O*, and OOH* intermediates adsorbed on the Fe site of the FeOOH model.

XVI. Structures of intermediates adsorbed on Fe and Co site in Co-FeOOH

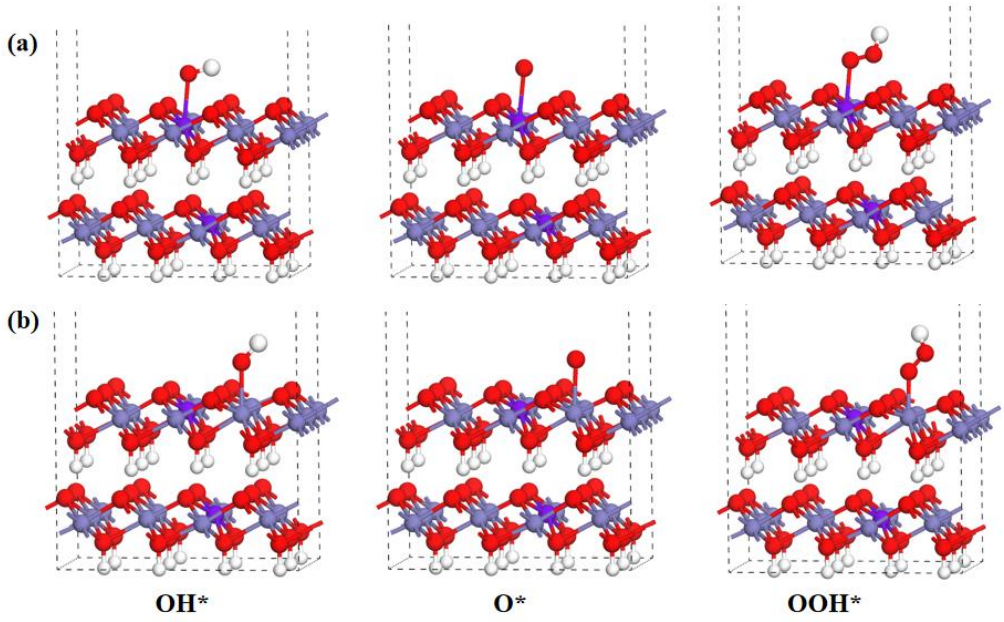

Figure S15. Structures of an OH*, O*, and OOH* intermediates adsorbed on the (a) Co and (b) Fe site of the Co-FeOOH model.

XVII. Structures of intermediates adsorbed on Fe and V site in V-FeOOH

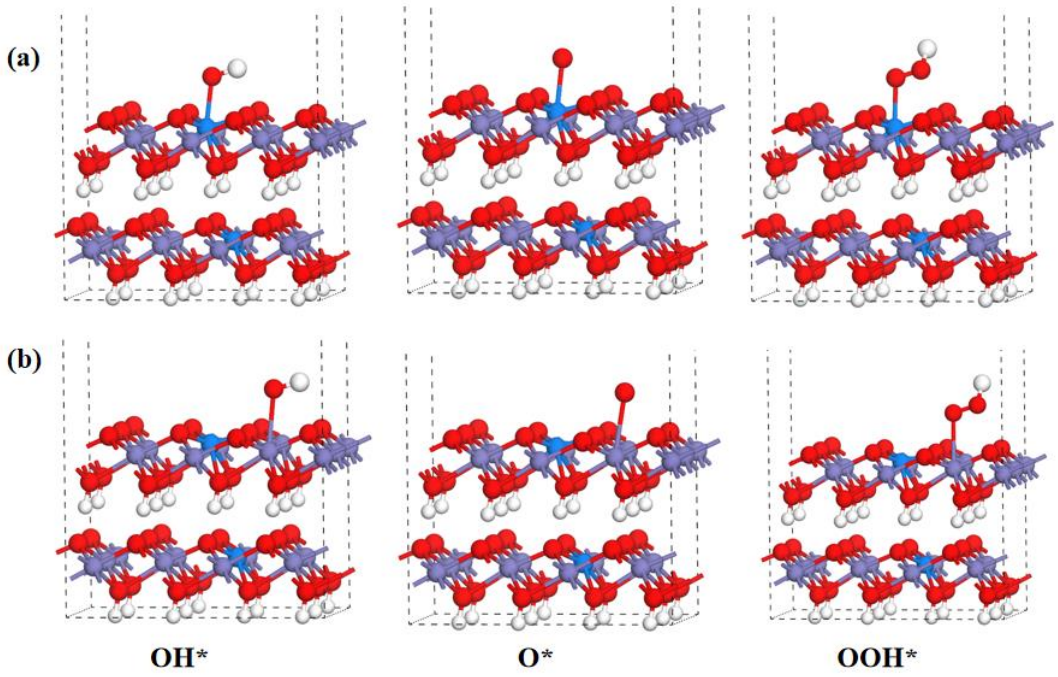

Figure S16. Structures of an OH*, O*, and OOH* intermediates adsorbed on the (a) V and (b) Fe site of the V-FeOOH model.

XVIII. Structures of intermediates adsorbed on Fe, Co and V site in (Co,V)-FeOOH

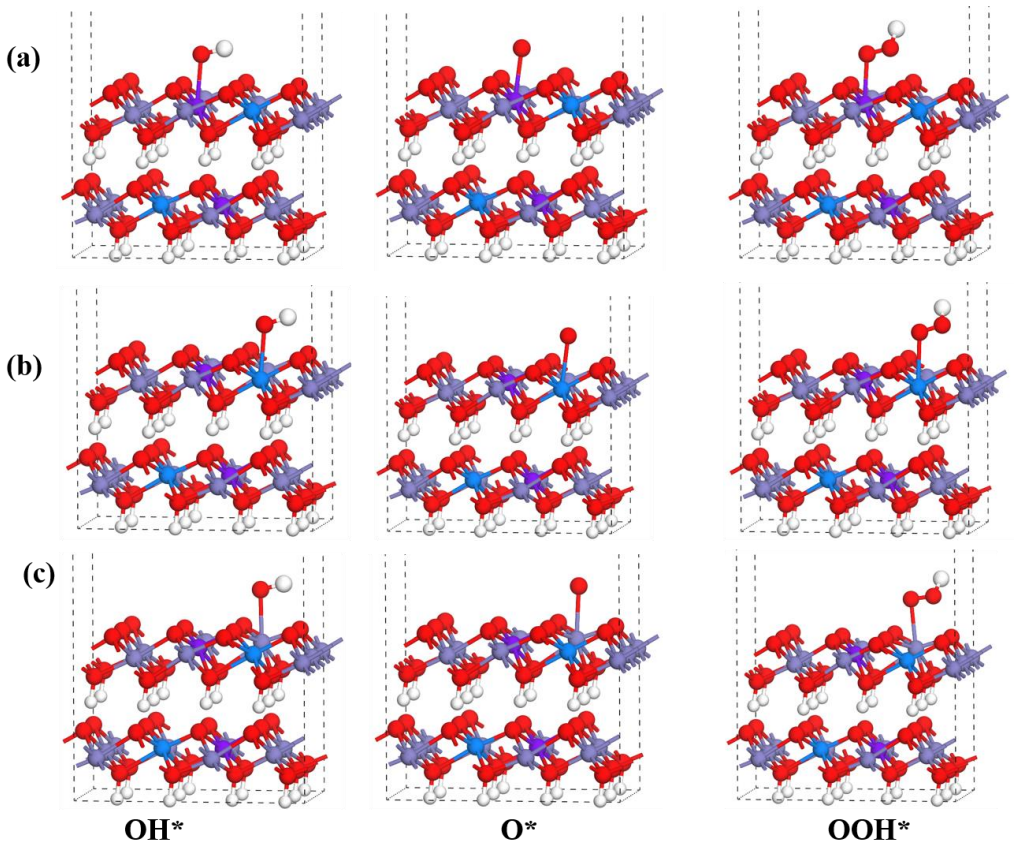

Figure S17. Structures of the OH*, O*, and OOH* intermediates adsorbed on the (a) Co, (b) V and (c) Fe site of the (Co,V)-FeOOH model.

XIX. Gibbs free energies of various metals in FeOOH and Co-FeOOH

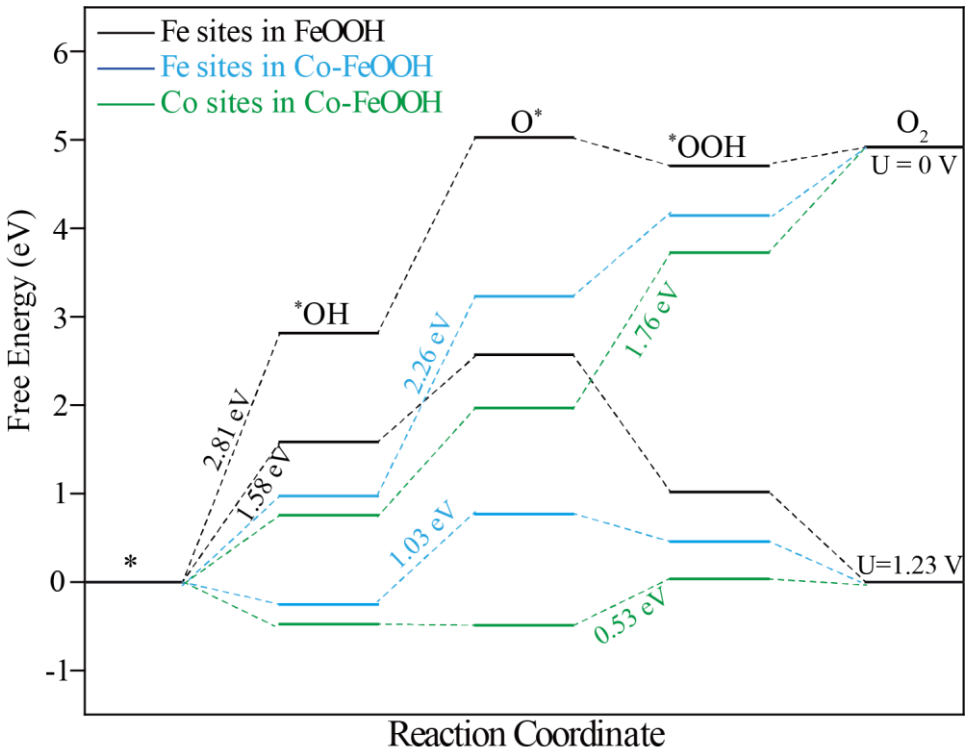

Figure S18. The free energies of Fe sites on the FeOOH model, Co and Fe sites on the Co-FeOOH model calculated at U=0 and 1.23 V, respectively.

XX. Gibbs free energies of various metals in FeOOH and V-FeOOH

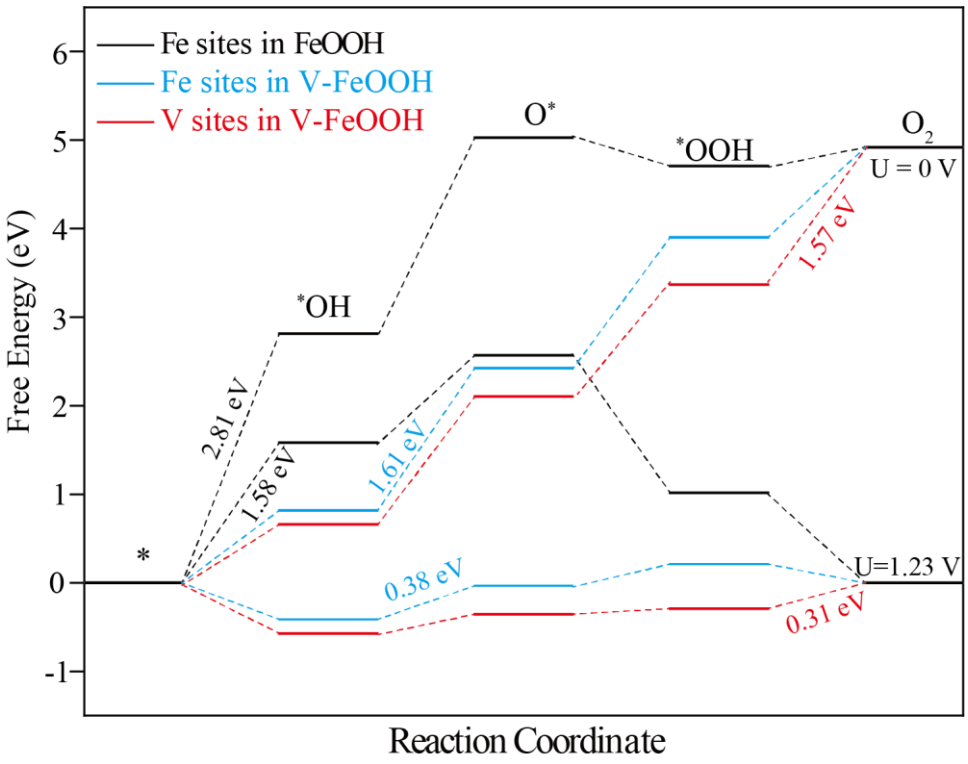

Figure S19. The free energies of Fe sites on the FeOOH model, V and Fe sites on the V-FeOOH model calculated at U=0 and 1.23 V, respectively.

XXI. Compare the OER activity of (Co,V)-FeOOH with other OER catalysts

Table S1. Comparison of the OER activities of (Co,V)-FeOOH with other non-noble metal based OER catalysts.

Catalysts	Electrolyte	Overpotentials at the corresponding j	Ref.
FeB_2	1 M KOH	η_{10} = 296 mV	S7
$FeSe_2$	1 M KOH	η_{10} = 245 mV	S8
FeOOH	1 M NaOH	η_{10} = 470 mV	S9
FeS_x	0.1 M KOH	η_{10} = 400 mV	S10
FeOOH(Se)/IF	1 M KOH	η_{10} = 287 mV η_{500} = 348 mV	S11
S-(Ni,Fe)OOH	1 M KOH + seawater	η_{500} = 398 mV	S12
$Ni_3Fe_{0.5}V_{0.5}$	1 M KOH	η_{100} = 264 mV η_{500} = 291 mV	S13
HG-NiFe	1 M KOH	η_{10} = 310 mV	S14
Ni–Fe–Se cages	1 M KOH	η_{10} = 240 mV	S15
$Fe_{0.5}V_{0.5}$	1 M KOH	η_{10} = 390 mV	S16
$Mo_{51}Ni_{40}Fe_9$	1 M KOH	η_{10} = 257 mV	S17
β-FeOOH:Ni/a-$Ni(OH)_2$	0.1 M KOH	η_{10} = 430 mV	S18
(Co,V)-FeOOH	1 M KOH	η_{10} = 230 mV η_{500} = 322 mV	**This work**

XXII. References:

[S1] D. Friebel, M. W. Louie, M. Bajdich, K. E. Sanwald, Y. Cai, A. M. Wise, M.-J. Cheng, D. Sokaras, T.-C. Weng, R. Alonso-Mori, R. C. Davis, J. R. Bargar, J. K. Nørskov, A. Nilsson, A. T. Bell, Identification of highly active Fe sites in (Ni, Fe) OOH for electrocatalytic water splitting. J. Am. Chem. Soc., 2015, 137, 1305-1313.

[S2] Kresse, G, Furthmüller, J. Efficiency of Ab-Initio total energy calculations for metals and semiconductors using a plane-wave basis set. Comput. Mater. Sci., 1996, 6, 15−50.

[S3] Kresse, G, Furthmüller, J. Efficient iterative schemes for Ab initio total-energy calculations using a plane-wave basis set. Phys. Rev. B, 1996, 54, 11169−11186.

[S4] Perdew, J. P, Burke, K, Ernzerhof, M., Generalized gradient approximation made simple. Phys. Rev. Lett., 1996, 77, 3865−3868.

[S5] Kresse, G, Joubert, D., From ultrasoft pseudopotentials to the projector augmented-save method. Phys. Rev. B, 1999, 59, 1758-1775.

[S6] Blöchl, P. E., Projector augmented-save method. Phys. Rev. B, 1994, 50, 17953−17979.

[S7] Hui Li, Peng Wen, Qi Li, Chaochao Dun, Junheng Xing, Chang Lu, Shiba Adhikari, Lin Jiang, David L. Carroll, Scott M. Geyer. Earth-abundant iron diboride (FeB_2) nanoparticles as highly active bifunctional electrocatalysts for overall water splitting. Adv. Energy Mater., 2017, 7, 1700513.

[S8] Chakadola Panda, Prashanth W. Menezes, Carsten Walter, Shenglai, Yao Matthias E. Miehlich, Vitaly Gutkin, Karsten Meyer, Matthias Driess, From a

molecular 2Fe-2Se precursor to a highly efficient iron diselenide electrocatalyst for overall water splitting. Angew. Chem. Int. Ed., 2017, 129, 10642 –10646.

[S9] Debarati Roy Chowdhury, Leone Spiccia, S. S. Amritphale, Amit Paul, Archana Singh, A robust iron oxyhydroxide water oxidation catalyst operating under near neutral and alkaline conditions. J. Mater. Chem. A, 2016, 4, 3655-3660.

[S10] Benjamin C. M. Martindale Erwin Reisner. Bi-functional iron-only electrodes for efficient water splitting with enhanced stability through in situ electrochemical regeneration. Adv. Energy Mater., 2016, 6, 1502095.

[S11] Shuai Niu, Wen-Jie Jiang, Zengxi Wei, Tang Tang, Jianmin Ma, Jin-Song Hu, Li-Jun Wan, Se-doping activates FeOOH for cost-effective and efficient electrochemical water oxidation, J. Am. Chem. Soc., 2019, 141, 17, 7005-7013.

[S12] Luo Yu, Libo Wu, Brian McElhenny, Shaowei Song, Dan Luo, Fanghao Zhang, Ying Yu, Shuo Chen, Zhifeng Ren, Ultrafast room-temperature synthesis of porous S-doped Ni/Fe (oxy)hydroxide electrodes for oxygen evolution catalysis in seawater splitting. Energy Environ. Sci., 2020, 13, 3439-3446.

[S13] Jian Jiang, Fanfei Sun, Si Zhou, Wei Hu, Hao Zhang, Jinchao Dong, Zheng Jiang , Jijun Zhao, Jianfeng Li, Wensheng Yan, Mei Wang, Atomic-level insight into super-efficient electrocatalytic oxygen evolution on iron and vanadium co-doped nickel (oxy)hydroxide. Nat. Commun., 2018, 9, 2885.

[S14] Jiong Wang, Liyong Gan, Wenyu Zhang, Yuecheng Peng, Hong Yu, Qingyu Yan, Xinghua Xia, Xin Wang, In situ formation of molecular Ni-Fe active sites on heteroatom-doped graphene as a heterogeneous electrocatalyst toward oxygen

evolution. Sci. Adv., 2018, 4, 7970.

[S15] Jianwei Nai, Yan Lu, Le Yu, Xin Wang, Xiong Wen (David) Lou, Formation of Ni-Fe mixed diselenide nanocages as a superior oxygen evolution electrocatalyst. Adv. Mater., 2017, 29, 1703870.

[S16] Ke Fan, Yongfei Ji, Haiyuan Zou, Jinfeng Zhang, Bicheng Zhu, Hong Chen, Quentin Daniel, Yi Luo, Jiaguo Yu, Licheng Sun, Hollow iron–vanadium composite spheres: A highly efficient iron-based water oxidation electrocatalyst without the need for nickel or cobalt. Angew. Chem. Int. Ed., 2017, 56, 3289 –3293.

[S17] Xiaoling Luo, Qi Shao, Yecan Pi, Xiaoqing Huang, Trimetallic molybdate nanobelts as active and stable electrocatalysts for oxygen evolution reaction. ACS Catal., 2019, 9, 1013–1018.

[S18] Tomiko M. Suzuki, Takamasa Nonaka, Kosuke Kitazumi, Naoko Takahashi, Satoru Kosaka, Yoriko Matsuoka, Keita Sekizawa, Akihiko Suda, Takeshi Morikawa, Highly enhanced electrochemical water oxidation reaction over hyperfine β-FeOOH(Cl):Ni nanorod electrode by modification with amorphous $Ni(OH)_2$. Bull. Chem. Soc. Jpn. 2018, 91, 778–786.